Colloid and Interface Science Communications 52 (2023) 100689

Contents lists available at ScienceDirect

Colloid and Interface Science Communications

journal homepage: www.elsevier.com/locate/colcom

Rapid Communication

Influence of the chemically reduced graphene oxide interface on the antioxidant multienzyme properties of Prussian blue nanoparticles

Yunong Zhang, Liubov Pershina, David Kudriashov, Andreas Offenhäusser, Yulia Mourzina *

Institute of Biological Information Processing (IBI-3 - Bioelectronics), Forschungszentrum Jülich, 52425 Jülich, Germany

ARTICLE INFO

Keywords:
Nanozyme
Prussian blue nanoparticles
Reduced graphene oxide
Multienzyme mimetics
Optical assay
Electrochemical sensor
Hydrogen peroxide
Superoxide radical anion
Catalase

ABSTRACT

Prussian blue nanoparticles (PB NPs) stabilized with surface capping agents as functional mimics of major antioxidant enzymes are attracting attention for use in reactions mediated by reactive oxygen species. However, influence of a stabilizing agent or interface on the enzyme-like properties of the nanomaterial remains unclear. In this study, we investigate the effect of the chemically reduced graphene oxide (rGO) interface on the morphology, stability, and multienzymatic activity of PB NPs. The rGO stabilized PB NPs nanocomposite (PB/rGO) demonstrated different morphology, dynamics of the superoxide scavenging, and lower peroxidase- and catalase-mimicking activities in comparison with the non-stabilized PB NPs. Electrochemical studies showed improved immobilization of PB/rGO on the graphite felt, while the sensitivity of hydrogen peroxide determination was higher for the non-stabilized PB NPs. This study enhances our understanding of the role of the rGO structuring interface in altering the properties of nanomaterials for oxidation protection and nanozyme-based sensing approaches.

Natural enzymes are powerful catalysts for specific biochemical reactions that proceed efficiently and specifically under extremely mild conditions. Natural enzymes also possess the potential for analytical applications, especially in the fields of electrochemical and optical sensing based on the peroxidase catalyzed oxidations. However, despite the intrinsic advantages of natural enzymes, researchers are trying to find substitutes because some shortcomings of natural enzymes limit their applications.

To overcome shortcomings such as poor stability, high cost of purification, and difficult synthesis, artificial enzymes have been studied and introduced [1,2]. Based on nanomaterials, nanozymes [3] are one of the aforementioned artificial enzyme mimics. Since the first discovery of Fe_3O_4 showing peroxidase-like activity, tremendous efforts have been devoted to research on nanozymes and nanomaterials with antioxidant activity [4–7]. Of all reported nanozymes, Prussian blue (PB) with a relatively high storage stability, low cost, and biocompatibility shows great catalytic activity and potential application value. Due to these advantages, there has been continuous progress in the development and use of PB nanozymes in analysis [8], for energy storage and conversion [9], environmental protection (detection and remediation of pollutants) [10,11], and as diagnostics and therapy agents in biomedicine [12], while minimizing the energy consumption and economic costs. As PB contains the $Fe(CN)_6^{4-}$ anion with Fe^{3+} cation, redox and corresponding optical changes controlled by the Fe(III/II) state enable the application of PB in both electrochemical and optical sensor systems. As reported in the literature, PB nanomaterials show significant (electro)catalytic activity for H_2O_2 reduction [13,14]. PB nanoparticles (PB NPs) have also been found to have multienzymatic activity of major antioxidant enzymes: peroxidase (POD), superoxide dismutase (SOD), and catalase (CAT) [14,15]. Thus, with all the advantages, PB NPs are considered a potential substitute for antioxidant enzymes in biotechnology and the analytical sciences [15,16]. Furthermore, PB NPs can be combined with additional materials to exploit synergistic effects in an attempt to enhance stability and influence other properties of the nanocomposites for various applications. Nevertheless, there is still a lack of knowledge about the multienzyme mimicking catalytic properties and low stability of PB nanomaterials and PB nanocomposites at biological pH.

Recently, low-dimensional carbon materials were used to create composites with metal hexacyanoferrates (MeHCFs), such as PB, to improve their properties [17]. These materials include graphene oxide (GO), rGO [18], carbon nanotubes (CNTs) [19], and carbon quantum dots (CQDs) [20]. Their applications range across different fields,

* Corresponding author at: Institute of Biological Information Processing (IBI-3, Bioelectronics), Forschungszentrum Jülich GmbH, Wilhelm-Johnen-Straße, 52428 Jülich, Germany.
E-mail address: y.mourzina@fz-juelich.de (Y. Mourzina).

https://doi.org/10.1016/j.colcom.2022.100689
Received 15 September 2022; Received in revised form 9 December 2022; Accepted 20 December 2022
Available online 24 December 2022

including radioactive waste treatment, biomedicine, and (bio)sensing [10,16]. These carbon materials are conductive, can promote electron transfer, and have good chemical stability. The presence of oxygen-containing groups in the graphene structure makes GO and rGO highly hydrophilic and capable of further functionalization and the synthesis of required composites. Oxygen-containing groups also act as stabilizing agents and prevent agglomeration [21,22]. In addition, carbon nanomaterials can increase the surface area of sensor systems, thus improving sensitivity and interactions between reaction components. Furthermore, it has been reported that modified carbon materials may possess enzyme-like activity and scavenge reactive oxygen species (ROS) [23,24]. Among several novel applications, graphene-based materials have been shown to possess antioxidant activity, i.e., they can act as radical scavengers against various ROS, in particular, for the superoxide radical anion [25]. On the other hand, it has been shown that various graphene and carbon nanomaterials exhibit very weak enzyme-like activity [23]. The primary free radical scavenging sites are associated with functional groups on graphene-based materials, doping with nitrogen and transition metals in the heteroatomic-doped carbon nanomaterials, sp^2-carbon network, and radical annihilation mechanism [23,24]. Nevertheless, the relative activity of low-dimensional carbon towards different ROS, as well as its effect as a structuring interface or stabilizing agent on the properties of the mixed-valence transition metal hexacyanoferrate (MeHCF) nanozymes has not been sufficiently explored or understood so far in optical or electrochemical assays, which motivates further research in this field aimed at creating efficient artificial enzymes.

Therefore, in this study, the properties of the non-stabilized PB NPs and PB/rGO nanocomposite are investigated and compared with the aim to establish the effect of the chemically reduced graphene oxide (rGO) stabilizing interface on the properties of nanozyme.

To study the intrinsic properties of PB NPs, PB NPs were synthesized from molecular precursors $FeCl_3$ and $K_3[Fe(CN)_6]$ through reduction with hydrogen peroxide and precipitation [14] without any stabilizing agent to exclude the influence of supporting substances. PB/rGO was prepared from molecular precursors $FeCl_3$, $K_3[Fe(CN)_6]$ and graphene oxide with ascorbic acid as a green reductant. All experimental details are provided in the Supporting information (section S1) and the methodology of the study is schematically presented in Fig. 1. This synthesis process allowed us to observe significant alteration of properties between PB NPs and PB/rGO nanomaterials. The average size of PB NPs in the synthesized non-stabilized PB NPs and PB/rGO nanocomposite was smaller than 100 nm (Figs. 2A, B and Fig. S1). The introduction of rGO did not create significant differences in the particle size. However, as shown in Figs. 2A, B and S1, the rGO matrix interface improved dispersion of the PB NPs in the PB/rGO nanocomposite, while PB NPs appeared agglomerated because of the absence of any stabilizing interface. The rGO surface decorated with the PB NPs is shown in Figs. 2A and S1A—C. More particles with a cubic-like structure were found in the PB/rGO samples (Figs. 2A and Fig. S1), while the boundaries and edges of the non-stabilized PB NPs (Figs. 2B and S1D—F) were less clearly defined. This difference can also be found in other studies, e.g. when PB was synthesized without any stabilizing agent, a sphere-like structure of PB was found by SEM [13], but cubic-like structures were found for the PVP-stabilized PB [15] and for the PB/rGO composite prepared by hydrothermal synthesis [10].

The XRD analysis (Fig. S2) showed that PB NPs in both samples were well-crystallized. The diffraction peak patterns were assigned to the face-centered cubic structure ($Fm^{-}3$ m) with unit cell dimensions of 10.152 Å and 10.194 Å for the PB NPs and PB/rGO, respectively. The difference in surface morphology of PB NPs and PB/rGO in SEM studies could be evidence of the role of the rGO interface, which indicates that PB NPs tend to aggregate, while rGO can inhibit the aggregation process by providing surface functional groups and consequently forming a stabilization interface. This indicates that rGO functions as a stabilizing agent.

The EDX analysis (Fig. 2C and Fig. S3) showed that the elements were uniformly distributed over the sample in both PB NPs and the PB/rGO-PB composite. Potassium ions were found in both samples, which agrees with the ICP-MS results (Fig. 2D and Table S1) and the XPS analysis (Fig. S4B). A higher fraction of potassium was found in the PB/rGO composite (Fig. 2D and Table S1), which can be explained by a generally high adsorption and intercalation of potassium ions into graphite and graphene materials [26]. Due to the higher mass fraction of potassium and presence of the rGO component, the mass fraction of the Fe catalytic sites in PB/rGO decreased by about 19% in comparison with PB NPs.

A comparison of the C1s spectra in the XPS analysis of GO and PB/rGO (Fig. S4) showed that the peak intensities of the oxidized carbon C—O at 287 eV, C═O at 288.3 eV, and O-C=O at 289.3 in PB/rGO decreased relative to the peak intensities of C—C and C—H at 285 eV in the PB/rGO, indicating the chemical reduction of GO to rGO in the PB/rGO composite [27].

The UV–vis spectra of the synthesized PB NPs and PB/rGO showed a characteristic PB absorbance band at about 700–800 nm with a maximum at about 750 nm (Figs. 2E and S5). No significant shift of the absorption was found between PB NPs and PB/rGO. Interestingly, the stability test showed a significantly higher stability of PB NPs in comparison with PB/rGO, especially at a biological pH value of 7.4 (Fig. 2F). While 98% and 56% of the initial PB absorbance at 750 nm remained for the PB NPs at pH 2 and pH 7.4 on day 10, respectively, the corresponding values decreased to 87% and 34% for the PB/rGO

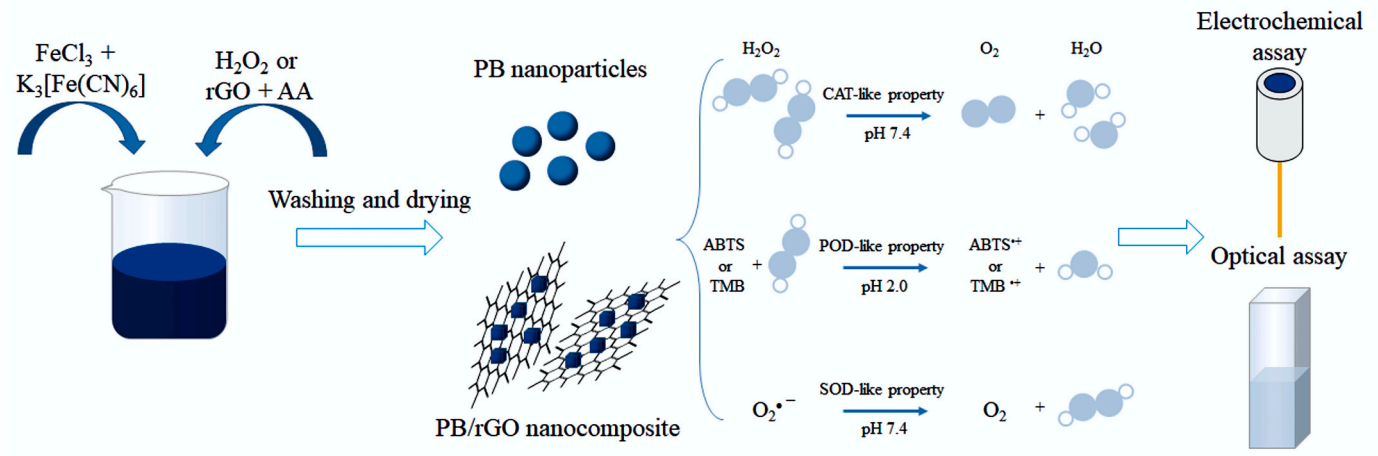

Fig. 1. Schematic diagram of the methodology of the study.

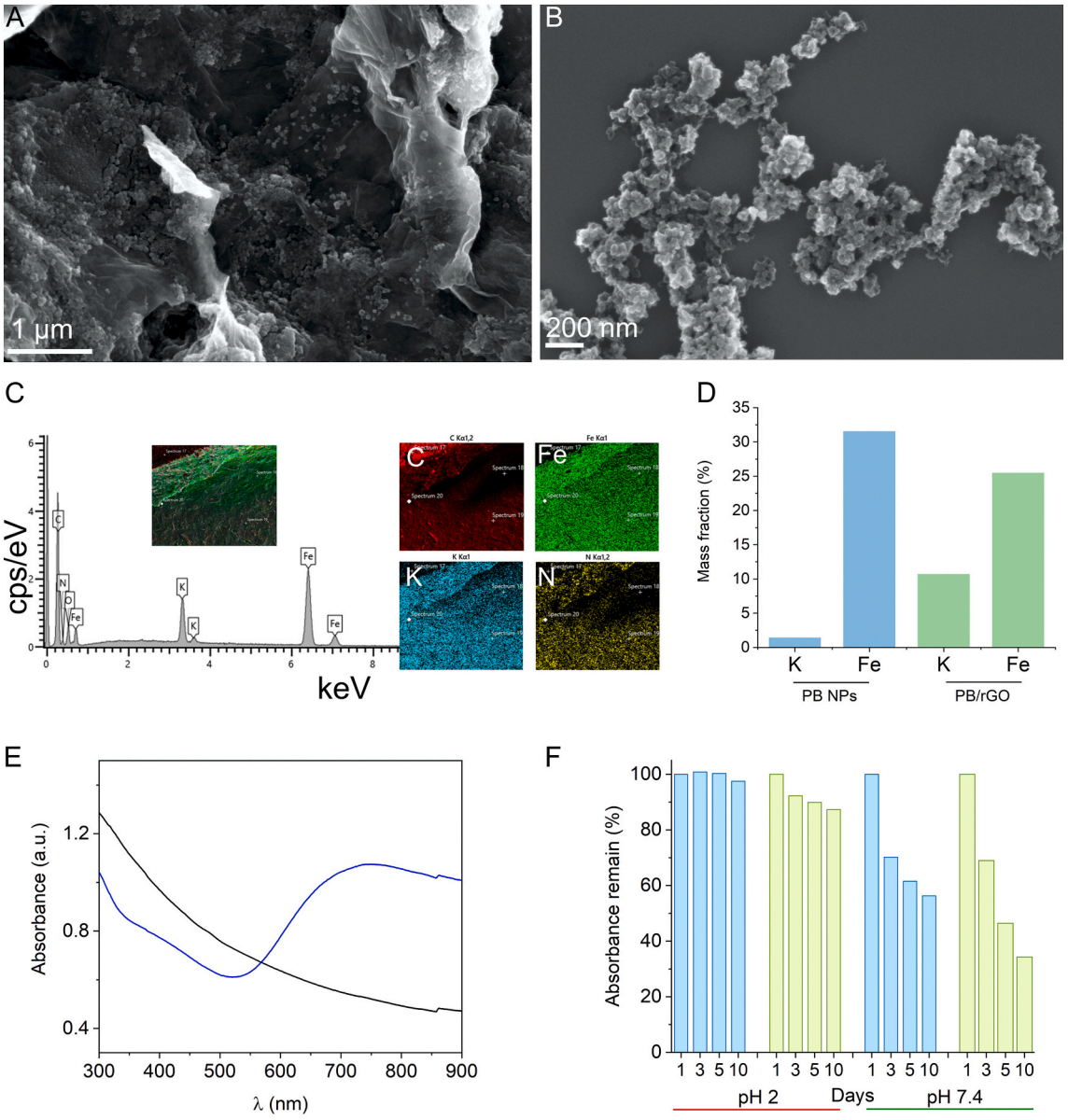

Fig. 2. SEM images of (A) PB/rGO nanocomposite and (B) PB NPs. (C) EDX analysis of PB/rGO. (D) Potassium and iron mass fraction diagram for PB NPs (blue) and PB/rGO (green): the mass fractions were found by ICP-OES. (E) UV–vis absorbance spectra of the GO before synthesis (black line) and PB/rGO composite at pH 2 (blue line). (F) Stability of the PB NPs (blue) and PB/rGO (green) at pH 2 and pH 7.4. (For interpretation of the references to colour in this figure legend, the reader is referred to the web version of this article.)

nanocomposite (Figs. 2F, S5B, and Table S2). This difference can be explained by a higher dispersion of the PB NPs in the PB/rGO nanocomposite than in the agglomerated PB NPs, as discussed above. As a consequence, a larger surface area of the PB NPs in the PB/rGO nanocomposite was available for contact with the solution, which resulted in a more extensive decomposition of PB NPs with precipitation of $Fe(OH)_3$ in the case of PB/rGO, especially at higher pH. Altogether, these data show influence of the rGO interface on the structural properties and stability of the PB NPs.

Biomimetic nanozyme activities of the PB/rGO nanocomposite were compared with those of PB NPs. Peroxidase-like activities were assessed through colorimetric assay using ABTS as a peroxidase donor substrate (see section S1.4). In this assay, the ABTS donor substrate can be catalytically oxidized by H_2O_2 in the presence of a nanozyme to produce $ABTS^{\bullet+}$ according to reaction (1):

$$2ABTS + H_2O_2 + 2H^+ \xrightarrow{nanozyme} 2H_2O + 2ABTS^{\bullet+} \quad (1)$$

The reaction can be easily monitored by measuring the absorption intensity change at 420 nm at optimum conditions [14]. As can be seen in Fig. 3A, the PB/rGO nanocomposite possessed enzyme-like activity, catalyzing the electron transfer between the substrate and H_2O_2. The catalytic activity of the rGO in the ABTS oxidation was found to be negligible (Fig. S6). This finding agrees with the results of Qui et al. [24]. Therefore, it can be concluded that the catalytic action of the PB/rGO nanozyme was due to the PB NPs component. The oxidation reaction kinetics obeyed the Michaelis-Menten model, which relates the reaction rate of the enzymatic reaction to the substrate concentration. Reaction rates became relatively stable after reaching the saturation concentration of the ABTS substrate. The parameters V_{max} and K_M were obtained by fitting the data from Fig. 3A using a Linewear-Burk plot, where V_{max} represents the maximal reaction rate of the enzymatic reaction at the

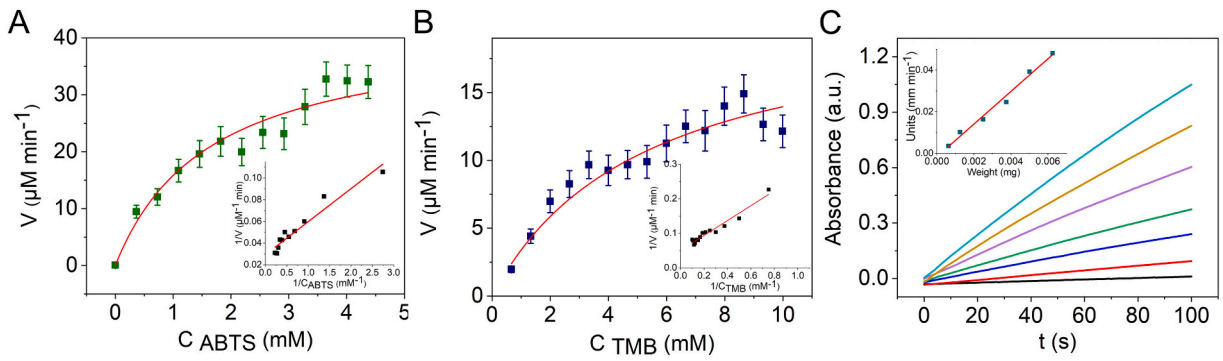

Fig. 3. Characterization of the catalytic kinetics of the PB/rGO nanocomposite with (A) ABTS substrate ($R^2 = 0.9129$, insert: $R^2 = 0.9251$) (see section S.1.4.1 for experimental details) and (B) TMB substrate ($R^2 = 0.9702$, insert: $R^2 = 0.9452$) (see section S.1.5 for experimental details). In (A) and (B), the nanozyme amount was 5 μg mL^{-1}. (C) Activity of 0, 0.5, 1, 2, 3, 4, 5 μg mL^{-1} PB/rGO nanocomposite with 3.6 mM ABTS, insert: $R^2 = 0.9829$ (see section S.1.4.2 for experimental details); insert shows the dependence of the activity on the weight of the nanocomposite.

saturated concentration of ABTS, and K_m represents the ABTS concentration at half of V_{max}. The K_m value is also a parameter that evaluates the affinity of a substrate to an enzyme. The results are listed in Table 1. The K_m^{ABTS} values of 0.68 mM [14] and 1 mM for the PB NPs and PB/rGO, respectively, indicated that the apparent affinity of the ABTS substrate to the PB NP nanozyme is lowered by the rGO in the PB/rGO composite. For comparison, the K_M of the ABTS substrate in the catalytic oxidation with a natural enzyme horseradish peroxidase is 0.66 at pH 4.2 [14]. The maximum reaction rate for the PB/rGO nanocomposite is about 90% of that for the PB NPs.

Furthermore, we found that another widely used peroxidase substrate TMB (section S.1.5) had a lower affinity to the nanozymes than ABTS. As can be seen in Table 1 and Figs. 3 A, B and S7, $K_M{}^{TMB}$ had much larger values than K_M^{ABTS} for both nanozymes.

Additionally, the specific peroxidase-like catalytic activity of the nanozymes, a^{POD}, [28] was found for the substrate with a higher affinity to the nanozyme (see section 1.4.2 and Fig. 3C). It can be seen in Fig. 3C that the absorbance increased slowly in the absence of nanozymes, indicating a moderate reaction between H_2O_2 and ABTS. When PB/rGO was added to the reaction mixture, the change rates of absorption increased, indicating an accelerated reaction rate between ABTS and H_2O_2. The data are summarized in Table 1. Although the weight fraction of the iron catalytic sites decreased in the PB/rGO nanocomposite in comparison with the PB NP nanozyme, the PB/rGO nanocomposite showed only a slightly lowered peroxidase-like catalytic activity (Table 1). This may be due to a facilitated contact of the reaction reagents, i.e. H_2O_2 oxidant and ABTS substrate, with the PB NPs surface in the PB/rGO nanocomposite because of a higher dispersion of the PB NPs in PB/rGO. This finding also indicates the ability of the rGO interface to influence on the peroxidase mimicking properties of PB NPs.

It has been reported that PB NPs have a poor peroxidase-like activity with increased pH values, and that they even become inactive in alkaline solution [14,15]. In neutral solutions containing H_2O_2 and PB NPs or PB/rGO nanocomposite, oxygen bubble formation was observed due to the emergence of the catalase-like activities, a^{CAT}, while catalase-like activity was not observed at pH 2. The catalase-like activities at higher pH values were evaluated by determining an initial rate of O_2 production in reaction (2) (see section S1.6 and Fig. 4A):

$$2H_2O_2 \rightarrow 2H_2O + O_2 \quad (2)$$

The a^{CAT} [29] was determined as the slope of the dependence of the observed rate constant of oxygen production, k_{obs}, on the concentration of the nanozymes (Fig. 4B). The comparison of the catalase activity of PB NPs and the rGO/PB nanocomposite (Table 1) showed that PB/rGO had a lower activity for catalyzing the decomposition of H_2O_2 than PB NPs, as evidenced by a smaller increase in the concentration of dissolved oxygen in the reaction mixture.

The peroxidase and catalase mimetic activities of PB NPs and the PB/rGO nanocomposite at different pH can be explained by the dependence on pH of the redox properties of hydrogen peroxide: hydrogen peroxide is a stronger oxidant at low pH [14]. Similar modulation of the enzyme-mimetic activities by changing the pH was recently found for the noble metals nanozymes [5].

Interestingly, there was a remarkable difference in the superoxide scavenging properties of the PB/rGO nanocomposite in comparison with PB NPs (Figs. 5A, B and S8). This was experimentally manifested in the difference of the inhibiting cyt c^{3+} reduction reaction with the enzymatically produced superoxide radical anion according to reaction (3) (see section S1.7 for experimental details):

$$\text{cyt } c^{3+} + O_2^{\bullet -} \rightarrow \text{cyt } c^{2+} + O_2 \quad (3)$$

The dynamics of the superoxide scavenging and cyt c^{3+} reduction observed for PB/rGO (Fig. 5A) differed significantly from those observed for PB NPs (Fig. S8 and 5B). In the latter case, an initial time delay, t_d, followed by a slower velocity of the cyt c^{3+} reduction was observed (Fig. S8). Fig. 5A shows that the reduction of cyt c^{3+} took place with a slower velocity in the presence of the PB/rGO nanocomposite, and was similar to the previously observed effects for soluble transition metal complexes [30] or SOD enzyme (Fig. 5C) that can be explained by the

Table 1
Biomimetic activity of the non-stabilized PB NPs and PB/rGO composite.

	Peroxidase-like activity ABTS				Catalase activity	$O_2^{\bullet -}$ scavenging activity[2]	
		K_M, mM	V_{max}, μM min^{-1}	a^{POD}, U μg^{-1}	a^{CAT}, μmol s^{-1} μg^{-1}	t_d, s	V/V_0 [3]
PB NPs	ABTS	0.68[1]	38[1]	7.2[1]	$2 \cdot 10^{-4}$ [1]	320 [1]	0.83 [1]
	TMB	9.4	117.5				
PB/rGO	ABTS	1.0	34.2	7.6	$1.2 \cdot 10^{-4}$	0	0.66
	TMB	9.2	30.9				

[1] Ref. [14].
[2] Found for nanozyme concentration of 50 μg mL^{-1}; [3] V - velocity of cyt c^{3+} reduction in the presence of nanomaterial after time delay; V_0 - velocity of cyt c^{3+} reduction in the absence of nanomaterials.

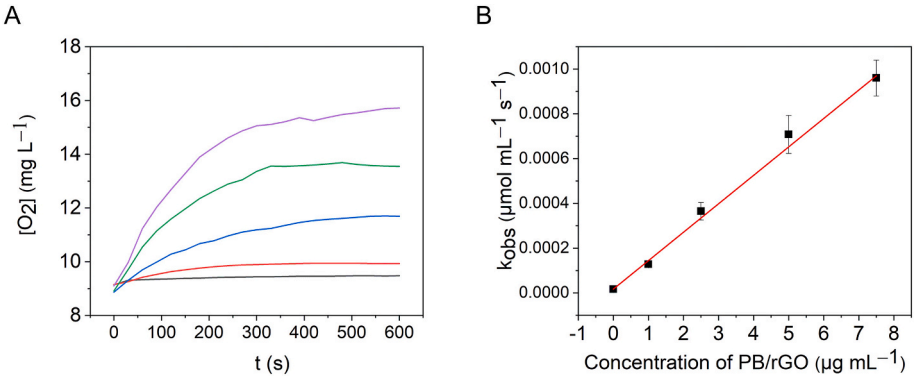

Fig. 4. (A) Dynamics of O_2 generation from 1.2 M H_2O_2 catalyzed by PB/rGO nanozyme at 25 °C in 0.1 M phosphate buffer, pH 7.4. (B) Dependence of the observed rate constant of oxygen production, k_{obs}, on the concentration of the PB/rGO nanozyme, where k_{obs} was determined as a rate of oxygen production in the initial 120 s anticipating zero-order reaction kinetics; $R^2 = 0.9901$.

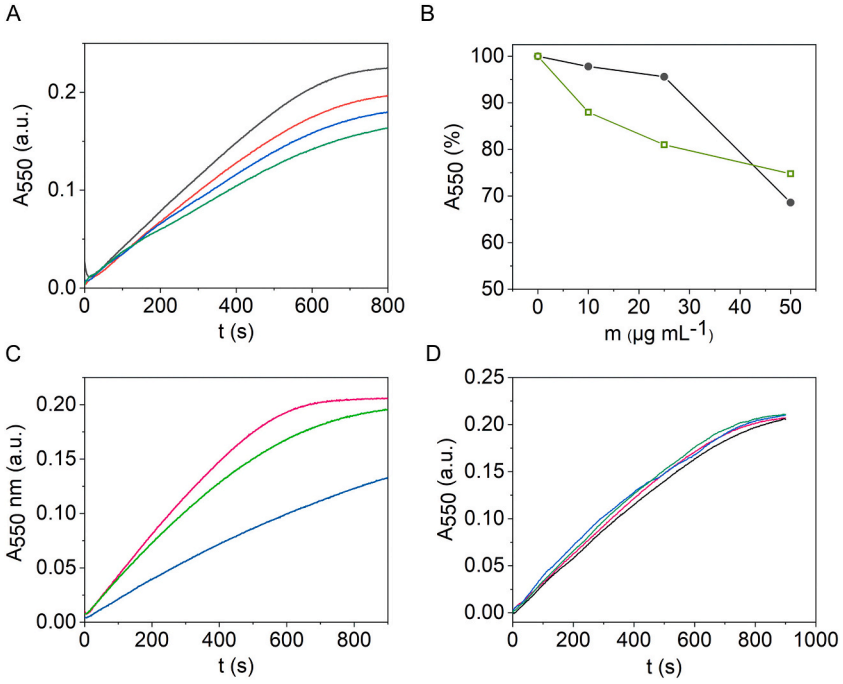

Fig. 5. (A) Reduction of cytochrome c^{3+} in the presence of 0 (black line), 10 (red line), 25 (blue line), and 50 (green line) µg mL^{-1} PB/rGO nanocomposite. (B) $A_{550}^{800\ s}$ absorbance in % after 800 s for the cytochrome c^{3+} reduction reaction in the presence of PB NPs (black line) and PB/rGO (green line). (C) Reduction of cytochrome c^{3+} in the presence of 0 (red line), 0.33 (green line), 1 (blue line) units mL^{-1} superoxide dismutase. (D) Reduction of cytochrome c^{3+} in the presence of 0 µg mL^{-1} (pink line) and 10 µg mL^{-1} of GO (black line), rGO (reduced with ascorbic acid similar to the preparation of the PB/rGO nanocomposite in section S1.4; blue line), and commercial rGO (green line). (For interpretation of the references to colour in this figure legend, the reader is referred to the web version of this article.)

following processes:

$$Fe^{3+} + O_2^{\bullet -} \rightarrow Fe^{2+} + O_2 \quad (4)$$

$$O_2^{\bullet -} \rightarrow H_2O_2 + O_2 \ \left(\text{fast disproportionation reaction, } k = 2{\cdot}10^5\ M^{-1}\ s^{-1}\right) \quad (5)$$

$$Fe^{2+} + H_2O_2 \rightarrow Fe^{3+} + OH^- + {}^{\bullet}OH \quad (6)$$

$$Fe^{x+} + xOH^- \rightarrow Fe(OH)_x \quad (7)$$

Previously, it was reported that rGO showed negligible peroxidase-mimetic activity but noticeable superoxide scavenging ability [24]. Other studies reported only limited catalytic activity of graphene or carbon-based nanozymes [23]. Therefore, we studied the influence of GO and rGO on cyt c^{3+} reduction to evaluate a possible contribution of these components to the superoxide scavenging properties of the PB/rGO nanocomposite. We found that GO and different rGO materials did not have a superoxide scavenging ability under the conditions of the experiment and cyt c^{3+} reduction remained unaffected by the presence of these compounds (Fig. 5D). Thus, we concluded that the superoxide scavenging ability of the PB/rGO nanocomposite was due to its PB component.

The difference in the $O_2^{\bullet -}$ scavenging properties and inhibition of the cyt c^{3+} reduction between PB NPs and the PB/rGO nanocomposite can be explained by taking into account differences in the morphology of these nanomaterials (Figs. 1,2). In the initial period, t_d, the inhibition of the cyt c^{3+} reduction was stronger for the PB NPs, because the enzymatically produced superoxide radical anion reduced most of the free Fe^{III} surface sites of the PB NPs in reaction (4). In contrast, the PB NPs in PB/rGO were randomly distributed and the rGO interface hindered contact between a short-lived superoxide radical anion and PB NPs in the nanocomposite to some extent and the superoxide radical anion could also reduce cyt c^{3+} in the initial period. In the case of PB NPs, after an initial period, the formation of the reduced form of PB, Prussian white (PW), and hydroxide layers on the surface of PB NPs according to reactions (4) and (7) hindered a further fast consumption of the superoxide radical anion by PB NPs and the reduction of cyt c^{3+} started. Thus, in the case of PB/rGO, diffusion through the rGO interface slowed down the reaction of $O_2^{\bullet -}$ with PB NPs in the nanocomposite and few Fe^{III} active site were consumed in the initial period. As a result, the inhibition

effect was more uniform. This property may be of interest for applications of the nanocomposite as a superoxide scavenger in biological systems.

Furthermore, the PB/PW redox cycle can be applied in electrochemical sensing to detect hydrogen peroxide and donor substrates of some oxidoreductases. Therefore, the electrochemical properties of the non-stabilized PB NPs and the PB/rGO nanocomposite were compared using a number of electrode materials: graphite felts electrodes (GFEs) and glassy carbon electrodes (GCEs). A quasi-reversible redox reaction of PB/PW was found (Fig. S9 and Table S3). According to the charge consumed in the PB/PW redox process, Q, (Table S3), despite the same amounts of pure non-stabilized PB NPs and of the PB/rGO nanocomposite as well as the same immobilization conditions, the amount of electroactive PB nanostructures immobilized on the GF and TGF electrodes was slightly larger for the PB/rGO nanocomposite although the PB/rGO had 20% fewer Fe $^{III/II}$ redox sites. This can be explained by better adsorption and conductivity of the PB/rGO nanocomposite on the graphite felt electrode material, as well as larger dispersion of the PB NPs in the PB/rGO, leading to a larger interface area between PB and the electrode material. Furthermore, the ratio $-Ip_c/Ip_a$ was close to 1 for the PB/rGO nanocomposite immobilized in graphite felt electrodes, while it was slightly higher for the PB NPs. In spite of favorable electrochemical characteristics, there was no sensitivity to hydrogen peroxide in a μM concentration range. We assume that hydrogen peroxide did not diffuse into the pores of hydrophobic GF or TGF, while PB did not adhere to the outer surface of GF and TGF.

PB/rGO-modified GCEs displayed two couples of redox peaks in CVs, similar to conventional PB-modified electrodes (Fig. S10) [14]. The peaks correspond to the PB/PW and BG/PB redox processes. The ΔE of the PB/PW redox processes were significantly smaller for the GCE-modified electrodes (Fig. S11 and Table 2) than for the modified graphite felt electrodes (Table S3) for both types of nanomaterials. Moreover, PB/rGO-modified GCE demonstrated characteristics of the redox process that were slightly closer to a reversible process, i.e. a value of ΔE close to a theoretical value of 59 mV and $-Ip_c/Ip_a$ close to 1, at both pHs. Electrochemical sensor properties based on the PB/PW cycle and the reduction of hydrogen peroxide at 0 V are shown in Fig. 6 and summarized in Table 2. For comparison, Fig. S12 illustrates that a non-modified bare GCE had no response to hydrogen peroxide at this potential in a concentration range below 1 mM. As follows from Table 2, the sensors based on PB NPs demonstrated slightly lower detection limits and higher sensitivities in both media, while the upper concentration working range of the PB/rGO nanozyme sensor material was similar or even slightly extended. Fig. 6 clearly illustrates that acidic media is more favorable for the sensor application of the PB/rGO nanozyme, because the sensors deteriorated after the concentration of H_2O_2 reached 1 mM at pH 7.4.

1. Conclusion

In conclusion, in this study, SEM, MS-ICP, and XRD analyses were carried out to study the influence of a chemically reduced graphene oxide interface on morphology of PB NPs. Optical method was used to study the differences in stability and mutienzyme activity between PB NPs and PB/rGO nanocomposite. It was found that the rGO interface resulted in a less agglomerated morphology and a better dispersion of PB NPs. But larger exposed surface area of PB NPs in PB/rGO nanocomposite caused lower stability. Compared with PB NPs, rGO showed negligible peroxidase-like activity, and PB/rGO nanocomposite showed reduced peroxidase-like activity in the oxidation of ABTS and TMB at the same experimental conditions, which demonstrated the ability of rGO interface to regulate the catalytic activities of PB NPs. Meanwhile, the results showed that PB NPs and PB/rGO extended the peroxidase catalyzed oxidations and assays to a lower pH range. Although cyano-bridged transition metal complexes are traditionally considered as "artificial peroxidase", our results highlight the "multifaceted" properties of these nanomaterials that based on the mimetic activity of three major antioxidant enzymes. The essentially different dynamics of superoxide scavenging between non-stabilized PB NPs and PB/rGO demonstrated a synergistic effect of two components in a material composite. Furthermore, electrochemical sensors based on GCE/(PB/rGO)/Nafion exhibited a lower sensitivity but a wider linear range up to higher concentrations of hydrogen peroxide at pH 7.4 in comparison with GCE/PB NPs/Nafion. It was found that using the PB/rGO nanocomposite led to a larger amount of electroactive PB nanostructures on the graphite felt electrodes in comparison with PB NPs in spite of approx. 20% fewer Fe $^{III/II}$ redox sites in the PB/rGO, which was brought by better adsorption and conductivity of the PB/rGO nanocomposite on the graphite felt electrode materials as well as larger dispersion of the PB NPs in the PB/rGO, leading to a larger interface area between PB and the electrode material. The results of this study not only reveal the role of the rGO structuring interface in altering the properties of MeHCF materials, but may also facilitate the design of other artificial enzymes. It is expected that higher performance of the transition metal complexes (TMC) nanozymes will be obtained with further continuous improvement in our understanding of the influence of synthesis, structural properties, stabilizing agents, and doping on their functional properties.

Author contributions

acquisition of data, analysis, writing, editing, Y.Z.; acquisition of data, analysis L.P. and D.K.; conception, analysis, A.O.; conception, design, supervision, analysis, interpretation of data, writing, review, editing, Y.M. All authors have read and agreed to the published version of the manuscript.

Funding

This research was supported by the China Scholarship Council, grant number 202008440365. The research was funded by the Deutsche Forschungsgemeinschaft (DFG, German Research Foundation) – 491111487.

Declaration of Competing Interest

The authors declare the following financial interests/personal relationships which may be considered as potential competing interests:

Yunong Zhang reports financial support was provided by Chinese Scholarship Council. Yulia Mourzina reports financial support was provided by Deutsche Forschungsgemeinschaft.

Table 2
Reversibility and analytical characteristics of the GCE/PB nanozyme/Nafion electrodes at pH 3 and pH 7.4.

		E_a [1], V	E_c [1], V	ΔE [1], V	$-I_{pc}/I_{pa}$ [1]	LDL, μM	Sensitivity, M $A^{-1}\cdot cm^{-1}$	Working concentration range, mM
GCE/PB-rGO/Nafion	pH 3	0.215	0.154	0.061	1.06	1.2	0.09	0.0012–5
	pH 7.4	0.214	0.160	0.054	1.00	6	0.06	0.006–1
GCE/PB NPs/Nafion	pH 3	0.216	0.105	0.111	1.05	1 [2]	0.23 [2]	0.001–5 [2]
	pH 7.4	0.235	0.168	0.067	1.16	3 [2]	0.11 [2]	0.003–0.7 [2]

[1] Found by cyclic voltammetry at 0.05 V s^{-1}; [2] ref. [14].

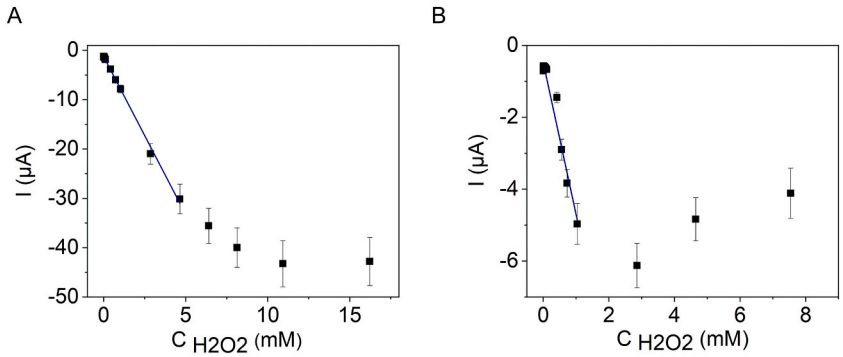

Fig. 6. Calibration curves of the GCE/(PB/rGO)/Nafion electrodes at (A) pH 3 ($R^2 = 0.9970$) and (B) pH 7.4 ($R^2 = 0.9609$) established by amperometry at 0 V.

Data availability

Data will be made available on request.

Acknowledgments

The authors would like to thank Dr. V. Nischwitz for the ICP-OES, Dr. E. Neumann and E. Brauweiler-Reuters for support with the structural analysis, and Dr. H. Hartmann and Dr. A. Besmehn for the XPS analysis.

Appendix A. Supplementary data

Supplementary data to this article can be found online at https://doi.org/10.1016/j.colcom.2022.100689.

References

[1] R.E. Breslow, Artificial Enzyms, John Wiley-VCH, Weinheim, Germany, 2006, p. 181.
[2] A. Bhattacharjee, V. Morya, C. Ghoroi, Enzyme-mimetic activity of sugar cane juice stabilized CuO nanospheres and CuO/GO nanocomposite: green synthesis and applications, Colloid Interface Sci. Commun. 35 (2020), 100239, https://doi.org/10.1016/j.colcom.2020.100239.
[3] F. Manea, F.B. Houillon, L. Pasquato, et al., Nanozymes: gold-nanoparticle-based transphosphorylation catalysts, Angew. Chem. Int. Ed. Eng. 43 (45) (2004) 6165–6169, https://doi.org/10.1002/anie.200460649.
[4] Q. Liu, A. Zhang, R. Wang, et al., A review on metal- and metal oxide-based nanozymes: properties, mechanisms, and applications, Nano-Micro Lett. 13 (1) (2021) 154, https://doi.org/10.1007/s40820-021-00674-8.
[5] E.L.S. Wong, K.Q. Vuong, E. Chow, Nanozymes for environmental pollutant monitoring and remediation, Sensors 21 (2) (2021) 408, https://doi.org/10.3390/s21020408.
[6] F. Gulbagca, S. Ozdemir, M. Gulcan, et al., Synthesis and characterization of Rosa canina-mediated biogenic silver nanoparticles for anti-oxidant, antibacterial, antifungal, and DNA cleavage activities, Heliyon 5 (12) (2019), e02980, https://doi.org/10.1016/j.heliyon.2019.e02980.
[7] F. Karimi, N. Rezaei-Savadkouhi, M. Ucar, et al., Efficient green photocatalyst of silver-based palladium nanoparticles for methyle orange photodegradation, investigation of lipid peroxidation inhibition, antimicrobial, and antioxidant activity, Food Chem. Toxicol. 169 (2022), 113406, https://doi.org/10.1016/j.fct.2022.113406.
[8] J. Estelrich, M.A. Busquets, Prussian blue: a nanozyme with versatile catalytic properties, Int. J. Mol. Sci. 22 (11) (2021) 5993, https://doi.org/10.3390/ijms22115993.
[9] X. Song, S. Song, D. Wang, et al., Prussian blue analogs and their derived nanomaterials for electrochemical energy storage and electrocatalysis, Small Methods 5 (4) (2021), e2001000, https://doi.org/10.1002/smtd.202001000.
[10] S.-C. Jang, Y. Haldorai, G.-W. Lee, et al., Porous three-dimensional graphene foam/Prussian blue composite for efficient removal of radioactive 137Cs, Sci. Rep. 5 (1) (2015) 17510, https://doi.org/10.1038/srep17510.
[11] B. Nayebi, K.P. Niavol, B. Nayebi, et al., Prussian blue-based nanostructured materials: catalytic applications for environmental remediation and energy conversion, Mol. Catal. 514 (2021), 111835, https://doi.org/10.1016/j.mcat.2021.111835.
[12] Z. Qin, Y. Li, N. Gu, Progress in applications of Prussian blue nanoparticles in biomedicine, Adv. Healthc. Mater. 7 (20) (2018) 1800347, https://doi.org/10.1002/adhm.201800347.
[13] M.A. Komkova, E.E. Karyakina, A.A. Karyakin, Catalytically synthesized Prussian blue nanoparticles defeating natural enzyme peroxidase, J. Am. Chem. Soc. 140 (36) (2018) 11302–11307, https://doi.org/10.1021/jacs.8b05223.
[14] Y. Zhang, D. Kudriashov, L. Pershina, et al., Intrinsic multienzyme-like activities of the nanoparticles of Mn and Fe cyano-bridged assemblies, Nanomaterials 12 (12) (2022) 2095, https://doi.org/10.3390/nano12122095.
[15] W. Zhang, S. Hu, J.-J. Yin, et al., Prussian blue nanoparticles as multienzyme mimetics and reactive oxygen species scavengers, J. Am. Chem. Soc. 138 (18) (2016) 5860–5865, https://doi.org/10.1021/jacs.5b12070.
[16] R.V. Blasques, J.S. Stefano, J.R. Camargo, et al., Disposable Prussian blue-anchored electrochemical sensor for enzymatic and non-enzymatic multi-analyte detection, Sens. Act. Rep. 4 (2022), 100118, https://doi.org/10.1016/j.snr.2022.100118.
[17] P.K. Lee, P.M. Woi, Current innovations of metal hexacyanoferrates-based nanocomposites toward electrochemical sensing: materials selection and synthesis methods, Crit. Rev. Anal. Chem. 50 (5) (2020) 393–404, https://doi.org/10.1080/10408347.2019.1642733.
[18] L. Cao, Y. Liu, B. Zhang, et al., In situ controllable growth of Prussian blue nanocubes on reduced graphene oxide: facile synthesis and their application as enhanced nanoelectrocatalyst for H2O2 reduction, ACS Appl. Mater. Interfaces 2 (8) (2010) 2339–2346, https://doi.org/10.1021/am100372m.
[19] T.-W. Chen, Z.-Q. Li, K. Wang, et al., Exploring the confinement effect of carbon nanotubes on the electrochemical properties of Prussian blue nanoparticles, Langmuir 34 (24) (2018) 6983–6990, https://doi.org/10.1021/acs.langmuir.7b03690.
[20] J. Chu, Y. Cheng, X. Li, et al., Prussian blue and carbon-dot hybrids for enhanced electrochromic performance, Materials 14 (12) (2021) 3166, https://doi.org/10.3390/ma14123166.
[21] J. Zhang, H. Yang, G. Shen, et al., Reduction of graphene oxide vial-ascorbic acid, Chem. Commun. 46 (7) (2010) 1112–1114, https://doi.org/10.1039/B917705A.
[22] S. Shah, N. Rangaraj, S.B. Singh, et al., Exploring the unexplored avenues of surface charge in nano-medicine, Colloid Interface Sci. Commun. 42 (2021), 100406, https://doi.org/10.1016/j.colcom.2021.100406.
[23] M. Liang, X. Yan, Nanozymes: from new concepts, mechanisms, and standards to applications, Acc. Chem. Res. (2019), https://doi.org/10.1021/acs.accounts.9b00140.
[24] Y. Qiu, Z. Wang, A.C.E. Owens, et al., Antioxidant chemistry of graphene-based materials and its role in oxidation protection technology, Nanoscale 6 (20) (2014) 11744–11755, https://doi.org/10.1039/C4NR03275F.
[25] G. Seber, J. Muñoz, S. Sandoval, et al., Synergistic exploitation of the superoxide scavenger properties of reduced graphene oxide and a trityl organic radical for the impedimetric sensing of xanthine, Adv. Mater. Interfaces 5 (2) (2018) 1701072, https://doi.org/10.1002/admi.201701072.
[26] J. Yang, Y. Yuan, G. Chen, First–principles study of potassium adsorption and diffusion on graphene, Mol. Phys. 118 (1) (2020), e1581291, https://doi.org/10.1080/00268976.2019.1581291.
[27] J. Feng, Y. Ye, M. Xiao, et al., Synthetic routes of the reduced graphene oxide, Chem. Pap. 74 (11) (2020) 3767–3783, https://doi.org/10.1007/s11696-020-01196-0.
[28] B. Jiang, D. Duan, L. Gao, et al., Standardized assays for determining the catalytic activity and kinetics of peroxidase-like nanozymes, Nat. Protoc. 13 (7) (2018) 1506–1520, https://doi.org/10.1038/s41596-018-0001-1.
[29] R. Kubota, S. Imamura, T. Shimizu, et al., Synthesis of water-soluble dinuclear Mn-porphyrin with multiple antioxidative activities, ACS Med. Chem. Lett. 5 (6) (2014) 639–643, https://doi.org/10.1021/ml400493f.
[30] Y.G. Mourzina, A. Offenhäusser, Electrochemical properties and biomimetic activity of water-soluble meso-substituted Mn(III) porphyrin complexes in the electrocatalytic reduction of hydrogen peroxide, J. Electroanal. Chem. 866 (2020), 114159, https://doi.org/10.1016/j.jelechem.2020.114159.